Raman studies of argon dimers in a supersonic expansion. I. Spectroscopy

H. P. Godfried* and Isaac F. Silvera*
Natuurkundig Laboratorium der Universiteit van Amsterdam, Valckenierstraat 65, 1018 XE Amsterdam, The Netherlands
(Received 13 August 1982)

Detection of argon dimers by means of Raman scattering is reported. This first observation of dimers by Raman scattering in a supersonic expansion provides a new technique for the study of the low-lying excitations of dimers and perhaps larger clusters, useful in determining interatomic potentials, etc. Spectra were recorded at low temperature and density in a supersonic expansion of pure argon. Both the pure rotational and the much weaker vibrational Raman transitions were observed for the lowest two vibrational states of the dimer. Raman transition frequencies were determined from the spectra. Theoretical spectra were generated with the use of the polarizability approximation. By using a classical point-dipole-induced dipole model in the calculation of the matrix elements and assuming a thermal distribution over the dimer levels, we could reproduce the rotational spectra to within experimental uncertainty.

I. INTRODUCTION

van der Waals molecules have been extensively studied since their discovery more than two decades ago.[1,2] These molecules are characterized by weak binding energies of order 10 meV for argon; for the extreme case of ^{3}He no bound state exists in the potential well. As a result, in a room-temperature gas they are present in such low concentrations that they are very difficult to detect. Two methods have been successfully applied for their study: (a) cooling the gas near the liquification temperature and (b) production in a supersonic expansion from a nozzle. In the latter case, downstream of the nozzle exit, the gas of the isentropic expansion cools sufficiently so that collisions result in the formation of dimers, trimers, etc.[3]

van der Waals (vdW) dimers of the rare gases have been studied mainly by two techniques: mass spectroscopy in a molecular beam and uv absorption in a cold stagnant gas. The study of the spectra provides detailed information concerning the interatomic potential. In addition, vdW dimers of molecules including species such as H_2, N_2, I_2, etc., can be made and have been studied by various other techniques such as infrared and fluorescence spectroscopy and magnetic resonance.[4] These spectra provide interesting new results concerning the (anisotropic) potentials and orientational configurations of these molecules. The technique of Raman scattering would be of substantial importance for studying the low-lying spectra arising from vibrational, rotational, librational, and tunneling excitations. In some cases due to symmetry, etc., Raman scattering is the only method of directly studying these low-lying spectra.

Recently, we succeeded in making the first successful observation of vdW molecules by spontaneous Raman scattering.[5] Earlier attempts by others[6,7] to measure these spectra in a stagnant gas were unsuccessful for a number of reasons. Such spectra are extremely weak since the intensity is proportional to the dimer density and to the square of the anisotropy in the polarizability. The latter arises from an induction mechanism in vdW molecules of rare-gas atoms and is typically small compared to the anisotropic polarizability of a covalent bonded molecule such as N_2.

To obtain a strong signal it would be desirable to have a large dimer density. At moderate temperature and pressure the dimer fraction is only of the order of 1% or less of the total gas density which must be kept low, otherwise the dimer spectra will be collisionally broadened. A further difficulty that arises in a high-density gas is a dominating overlapping spectrum due to collision-induced scattering from unbound pairs of atoms. Finally, even for low densities, the spectra which can lie at very small frequency shifts from the laser frequency suffer from interference with the strong Rayleigh and parasitic scattering intensities.

In this and an accompanying article an extensive description is given of our Raman scattering experiments on Ar_2 in a supersonic expansion. In this paper attention will be focused mainly on the spectroscopic results of the experiments. The second arti-

cle, to be referred to as II, will discuss some of the properties of the expansion, the gas kinetic aspects of the dimer formation, and the relaxation of its internal degrees of freedom.

An expansion was used in order to increase the dimer signal and to simplify interpretation of the spectra: The dimer fraction increases in the expansion since, due to the cooling, the chemical equilibrium between dimers and monomers shifts to the dimers. Although collisions are needed to obtain the increase, the density falls so rapidly that collisional broadening is unimportant except near the nozzle throat. In addition, collision-induced light scattering is negligible. Nevertheless, there is a sufficiently high collision rate so that the dimers can cool along with the monomers down to low temperatures. We have studied Ar_2 for $T \simeq 30$–40 K, far below argon's triple point of 83.8 K. A further spectroscopic simplification results since only a limited number of states are thermally populated.

The article is organized as follows. In Sec. II spectroscopy of argon dimers is discussed. The earlier spectroscopic work is first reviewed; then Raman scattering theory is applied to Ar_2. The argon diatom polarizability is discussed and, finally, linewidth calculations are presented. The experimental technique is described in Sec. III. In Sec. IV a brief introduction into expansion theory is given. In Sec. V the dimer spectra are presented. Finally, a short summary of results is given in Sec. VI.

II. ARGON-DIMER SPECTROSCOPY

A. Review of earlier work

Molecular absorption bands of Ar_2 were first recorded by Tanaka and Yoshino[8] in the vacuum ultraviolet. Since they could only resolve the vibrational structure of the ground-state molecules their experiments were subsequently repeated by Colbourn and Douglas[9] with improved apparatus. In one band system these authors were able to resolve the rotational structure of the ground electronic state. Using their spectroscopic data and high-temperature viscosity data of Maitland and Smith,[10] Chen and Aziz[11] constructed a potential, called HFD-C, that could fit most of the available data on virial coefficients and transport properties and also seems to agree with more recent scattering experiments.[12] The potential reproduces the spectroscopic levels of Colbourn and Douglas (CD) to approximately 0.2 cm^{-1}. For most of the bound levels the agreement is almost an order of magnitude better. It also predicts the metastable levels, though with reduced accuracy. In the rest of this article this potential will be used in calculations unless noted differently.

B. Raman spectroscopy of argon dimers

The Raman scattering efficiency is given in the polarizability approximation of Placzek and Teller[13] by

$$S = r' \nu \nu'^3 \, | \alpha_{if}^2 | \, \rho_i \delta(E_{if} - h(\nu' - \nu)) \ , \tag{2.1}$$

where ν and ν' are the incident and scattered light frequencies, respectively. α_{if} is the polarizability matrix element between initial and final states and r' contains some numerical factors. ρ_i is the density of scatterers in the initial state and the δ function serves to conserve energy, with E_{if} the difference in energy between the initial and final states. The efficiency S is the number of scattered photons per incident photon, per unit frequency, per unit solid angle, per unit sample length. The matrix element squared $|\alpha_{if}|^2$ is proportional to

$$| \langle \chi_{v'J'}(R) | \alpha^{\mathrm{mol}}(R) | \chi_{vJ}(R) \rangle |^2 \ , \tag{2.2}$$

where $\alpha^{\mathrm{mol}}(R)$ is the diatom polarizability in the molecular frame and the initial [final] state $\chi_{vJ}(R)$ [$\chi_{v'J'}(R)$] is a solution of the radial Schrödinger equation for the diatomic system:

$$\left[-\frac{\hbar^2}{2m} \frac{d^2}{dR^2} + V(R) + \frac{\hbar^2 J(J+1)}{2mR^2} \right] \chi_{vJ}(R) = E_{vJ} \chi_{vJ}(R) \ . \tag{2.3}$$

Here v,J denote the vibrational and angular momentum quantum numbers. After separating out the angle-dependent factors, averaging over the polarizations of the incident and scattered light and summing over magnetic sublevels[14] we get for the Raman scattering efficiency

$$S \propto \nu \nu'^3 S_J \, | \langle \chi_{v'J'} | \alpha^{\mathrm{mol}} | \chi_{vJ} \rangle |^2 \times \rho_{vJ} \delta(E_{if} - h(\nu' - \nu)) \tag{2.4}$$

with S_J a J-dependent factor and $\rho_{vJ} \equiv \rho_i$ the density of scatterers in the initial state with quantum numbers v,J. For Ar_2, as a spinless homonuclear diatomic molecule, the usual Raman selection rules apply: $\Delta J = 0, \pm 2$. S_J is given by (for S-, Q-, and O-branch transitions, respectively)

$$S_J = \begin{cases} \frac{3}{2} \frac{(J+1)(J+2)}{(2J+1)(2J+3)} & (\Delta J = +2) \quad (2.5a) \\ \frac{J(J+1)}{(2J-1)(2J+3)} & (\Delta J = 0) \quad (2.5b) \\ \frac{3}{2} \frac{J(J-1)}{(2J-1)(2J+1)} & (\Delta J = -2) \ . \quad (2.5c) \end{cases}$$

Owing to nuclear-spin statistics only even J states are allowed for the dimer in its ground electronic state $^1\Sigma_g^+$. Owing to the shallowness of the potential, the dimer wave functions probe a large range of the attractive well. Therefore, anharmonicity in the potential and centrifugal distortion strongly affect the energies of the dimer levels. As a consequence, a rotational Raman spectrum consisting of sets of only approximately equally spaced lines (spacing is $\simeq 8B_v$ where $B_v=\hbar^2/2mR^2$ is the rotational constant) for each of the vibrational states is expected. The vibrational-rotational spectra are expected to show a structure with a high density of states at the bandhead in the S and Q branches due to the differences in the rotational constants of the different vibrational states and the increasing effects of anharmonicity.

C. Diatom polarizability

In order to predict the intensity of the dimer Raman spectra, expression (2.2) has to be evaluated within some model for the diatom polarizability. A vast number of collision-induced light scattering measurements of the polarizability have been presented in the literature.[6(b),15,16] The results were mostly at variance with one another. Recently, however, most of the experiments indicate that a classical point-dipole-induced dipole (DID) model adequately describes the data.[16,17] This is supported by recent theoretical calculations.[18] In the discussion in this section we will concentrate on the DID model, but later on, results of other models will be compared to experiment. Working in the molecular frame one finds for the DID model.[19]

$$\beta(R)=\frac{6\alpha_0^2}{R^3}+\frac{6\alpha_0^3}{R^6}+O(R^{-9}) \tag{2.6a}$$

and

$$\tfrac{1}{3}\,\mathrm{Tr}\Delta\alpha(R)=\frac{A_6}{R^6}+O(R^{-9}) \tag{2.6b}$$

with $\alpha_0=11.34$ a.u. and $A_6=9665$ a.u. $\beta(R)\equiv\alpha_{||}-\alpha_\perp$ is the (incremental) anisotropy in the diatom polarizability in the molecular frame, R the internuclear distance, and α_0 the atomic polarizability. The trace polarizability [Eq. (2.6b)] is not strictly the DID result but has been corrected for correlation effects.[20]

Matrix elements of β for bound dimer states have been reported by Frommhold.[7] His calculations were initially carried out using approximate wave functions. In a later comment,[21] matrix elements were computed with the v- and J-dependent solutions of the radial Schrödinger equation [Eq. (2.3)]. The potential used was the MSVIII potential.[22] Only a few representative matrix elements were given and these seem to have a numerical error of approximately a factor of 3. (This may be due to an incorrect numerical factor in their formula for the DID result for β.)[23] The matrix elements were therefore recalculated in the present work. For S transitions ($J'-J=+2$) the results are shown in Fig. 1 as a function of initial angular momentum J of the dimer. The pure rotational transitions ($\Delta v=0$) are seen to be about an order of magnitude larger than the vibrational terms. Contribution of the second term in Eq. (2.6a) ($\propto R^{-6}$) is about 3% of the total; it is fairly independent of v or J. For the vibrational matrix elements the R^{-6} term contribution varies as a function of v and J between 5% and 10% of the main term. In view of its smallness with respect to the R^{-3} term we have neglected the quantum corrections to it which, similar to the isotropic polarizability, are due to correlations.[20(b)] The Q- and O-branch matrix elements are generally somewhat smaller than the S-branch elements with the same initial state. Q-branch transitions also get a contribution from the isotropic scattering [Eq. (2.6b)]. This is found to be negligible.

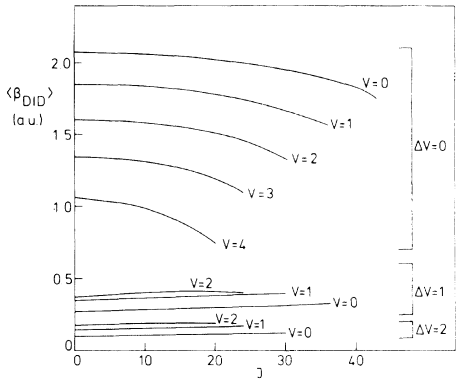

FIG. 1. Radial anisotropic polarizability matrix elements for the dipole-induced dipole model in atomic units as a function of the initial rotational quantum number J for Stokes S transitions [Eq. (2.2) with $J'=J+2$ and $v'\geq v$]. Different curves correspond to different values of the initial vibrational quantum number v and of $\Delta v=v'-v$, the change in vibrational quantum number. Curves marked $\Delta v=0$ correspond to the pure rotational Raman transitions. Geometrical factors S_J [Eq. (2.5a)] are not included.

D. Dimer linewidths

In Eqs. (2.1) and (2.5) the energy-conserving delta function should, in fact, be replaced by some physical line-shape function that reflects the width of the Raman lines. Apart from the finite width of the exciting laser, the main contribution for the bound dimer states comes from collisional line broadening.

For the metastable states tunneling through the rotational barrier may also be of importance.

Collisional broadening has been discussed by Frenkel and McTague[24] in a semiclassical approximation based on the work of Gordon[25] on collisional linewidths. In this method the equations of motion are solved classically for a collision between a dimer and a monomer. The line-broadening cross section σ_{ii} for the ith Raman line is given by

$$\sigma_{ii}=\langle v_{\rm rel}\rangle^{-1}\int_0^\infty 2\pi b\,db\,\langle v_{\rm rel}\sigma_{ii}(b,v_{\rm rel})\rangle \ , \tag{2.7}$$

where $v_{\rm rel}$ is the relative velocity between the collision partners. The brackets $\langle\ \rangle$ indicate a thermal average and the integral is over all impact parameters b. The cross section $\sigma_{ii}(b,v_{\rm rel})$ is given semiclassically for Stokes and anti–Stokes-Raman transitions by

$$\sigma_{ii}(b,v_{\rm rel})=1-P_{ii}\cos^4(\alpha/2)\exp(\pm 2i\eta) \tag{2.8}$$

with P_{ii} the probability that a collision is elastic, α the reorientation angle of the angular momentum, and η the collisional phase shift of the rotor. The linewidth of the ith Raman line is then found as

$$\Delta\nu_{1/2}=\rho\langle v_{\rm rel}\rangle\sigma_{ii}/2\pi \tag{2.9}$$

with ρ the density. For most of the interesting transitions these authors found $\sigma_{ii}\simeq 200$ Å^2 at $T=143$ K. The temperature dependence was found to be weak, $\sigma\sim T^{-0.13}$. For our conditions in the expansion ($\rho\simeq 0.5$ amagat, $T\simeq 40$ K, $\Delta\nu_{1/2}\simeq 0.03$ cm^{-1} which is smaller than the instrumental resolution.

TABLE I. Dimer linewidth calculations. Columns 1,2: vibrational and rotational quantum numbers of states. Column 3: energies of states relative to lowest vibrational-rotational state (Ref. 9). Column 4: results of JWKB calculation of tunneling width in cm^{-1}; since the state with $v=0$ and $J=30$ is stable, its tunneling width is 0. Column 5: results of collisional Raman linewidth calculation in cm^{-1} for pure rotational Stokes-Raman transitions at $T=39$ K and $\rho=0.5$ amagat; only collisions between dimers and monomers are included in the calculation. Column 6: dimer level width due to inelastic collisions in cm^{-1}; this is discussed in paper II.

v	J	E (cm^{-1})	Tunneling width (cm^{-1})	Raman width (cm^{-1})	Coll. width (cm^{-1})
0	30	52.76	0	0.022	0.015
0	40	91.60	0.24×10^{-26}	0.022	
0	42	100.44	0.62×10^{-15}		
0	44	109.60	0.26×10^{-9}		
0	46	119.05	0.88×10^{-6}	0.022	
0	48	128.74	0.24×10^{-3}		
1	34	86.91	0.15×10^{-32}		
1	36	93.83	0.28×10^{-14}	0.024	
1	38	101.03	0.66×10^{-8}		
1	40	108.45	0.26×10^{-4}	0.023	
1	42	116.04	0.53×10^{-2}	0.022	
2	30	89.21	0.21×10^{-14}	0.027	0.019
2	32	94.64	0.93×10^{-7}		
2	34	100.23	0.42×10^{-3}		
*2	36	105.88	0.52×10^{-1}	0.028	
*2	38	111.45	0.62		
3	24	86.18	0.55×10^{-17}		
3	26	90.00	0.48×10^{-6}	0.029	
3	28	93.94	0.30×10^{-2}		
*3	30	97.84	0.19		0.021
4	20	86.90	0.43×10^{-6}		
4	22	89.43	0.87×10^{-2}		
5	16	86.56	0.84×10^{-2}		

Therefore, it is not pursued any further for the bound states.

For the metastable states the natural width due to tunneling was calculated using the JWKB method.[26] In this semiclassical method the predissociation lifetime τ is given as the ratio of the oscillation period t_{vib} within the potential well to the probability ω of transmission through the barrier. Thus the linewidth is given as[27]

$$\Delta\nu_{1/2}=\frac{1}{2\pi\tau}=\frac{1}{2\pi}\frac{\omega}{t_{\text{vib}}} \tag{2.10}$$

with

$$\omega=\exp\left[-\frac{(8\mu)^{1/2}}{\hbar^2}\int_{R_2(E)}^{R_3(E)}[U(R)-E]^{1/2}dR\right], \tag{2.11}$$

$$t_{\text{vib}}=(2\mu)^{1/2}\int_{R_1(E)}^{R_2(E)}[E-U(R)]^{-1/2}dR \ . \tag{2.12}$$

Here $R_1(E)<R_2(E)<R_3(E)$ are the classical turning points for the system at the resonance energy E with effective potential energy (that is, including the centrifugal term) $U(R)$. The integrals for t_{vib} and ω are thus calculated in the classically allowed region within the well and in the forbidden region, respectively (Table I). The values for the linewidth, given in column 4, were calculated at the resonance energies given by Colbourn and Douglas with the use of the HFD-C potential. Since this potential gives slightly different resonance energies the width was also calculated at those resonances. Results differed approximately 20%. It is to be noted that for the smallest linewidths slight changes in the potential easily change the width by an order of magnitude. For a particular choice of the potential, however, the JWKB method is expected to give fairly accurate results, especially for the narrow linewidths that are found in a heavy system such as Ar_2.[27] In column 5 of Table I the Raman linewidths [Eq. (2.9)] are given. These linewidths then also dominate for most of the metastable states with the exception of those indicated by *.

III. EXPERIMENTAL

A schematic of the experimental apparatus is shown in Fig. 2. In order to obtain a large Raman signal we used a crossed intracavity laser-expansion geometry somewhat modified from our earlier design which used an internal focusing lens.[28] The laser cavity was formed by three mirrors (M1, M2, and M3) in a folded configuration to produce a focus of 10-μm diameter crossing the expansion axis at right angles. The radius of curvature of M_1 was

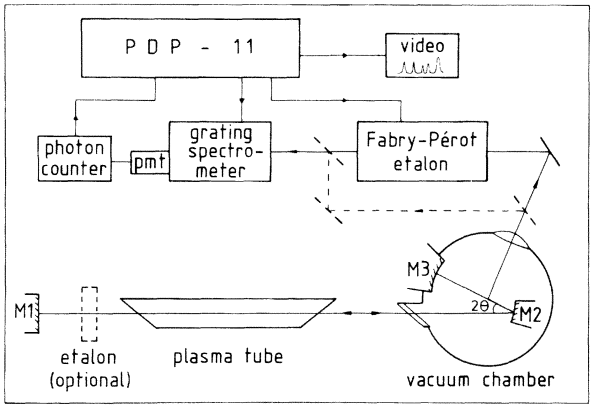

FIG. 2. Schematic of the experimental apparatus. Expansion nozzle (not shown) is centered in the vacuum chamber with its axis pointing out of the page.

∞; those of M_2 and M_3 were 50 mm. The folding angle was kept as small as possible ($2\theta\sim5°$) to minimize astigmatism. An intracavity power of the order of 50 W was achieved with the use of a Spectra Physics 166 Ar^+ laser with a nominal power of 1.8 W in conventional operation. An optional intracavity etalon narrowed the 5-GHz laser linewidth down to about 0.5 GHz, at the expense of a factor of 2 in power. The laser then resonated in approximately three longitudinal modes. This had the advantage of improved amplitude stability over single-mode operation, while the resultant laser width was still substantially narrower than the spectrometer system resolution.

Raman scattered light was collected at right angles to both the laser and expansion axes. To observe the closely spaced rotational transitions the necessary high resolution was obtained using a Burleigh RC-10 Fabry-Perot etalon that was driven and actively stabilized with an on-line Digital Equipment Corporation PDP-11 computer. This was scanned in tandem with a Jobin-Yvon HG2S grating spectrometer with a bandpass of approximately 2 cm^{-1} which served to reject the large interfering Rayleigh signal. The etalon was operated with a free spectral range of 6.9 cm^{-1} and finesse of ~75. Resolution was 0.09 cm^{-1} with the intracavity etalon and 0.18 cm^{-1} without it. Because of the expected weakness of the vibrational spectra no attempt was made to resolve the individual transitions. Instead, a direct optical path circumventing the Fabry-Perot etalon was used to reduce the losses. Resolution was then approximately 1 cm^{-1}.

For detection of scattered light a cooled ITT FW130 photomultiplier (PMT in the figure) with a 0.8-Hz dark count was used along with digital photon counting. Spectra were stored and averaged by

the computer. The system was stable for about 20 hours, being limited by a deterioration of the intracavity power. A high-resolution run required about 1 hr/cm^{-1} measurement time. All spectra were recorded on the Stokes side of the laser line.

Before or after measurements of argon spectra, a known Raman spectrum was recorded for frequency calibration of the spectrometer system. Gases used were CO_2 when recording rotational dimer spectra, and N_2 and/or O_2 for the vibrational spectra. From the CO_2 calibration spectra we detected some nonlinearity in the piezoelectric drive of the Fabry-Perot etalon. In addition, creep of the piezoelectric transducers distorted the frequency scale. Creep effects were most noticeable after the piezoelectric transducers had been rapidly reset to their initial position for multiscan averaging. Details of the nozzle and gas handling system will be given in paper II.

IV. EXPANSION

Although the expansion properties will be considered in detail in paper II, it is useful to give a short introduction into expansion theory to characterize the state of the system. In the expansion the random thermal motion of the expanding gas particles is converted to directed mass flow via interparticle collisions. This then causes the cooling of the gas; very low temperatures can be achieved this way. The consequences this has for the dimer spectra have been mentioned in the introduction.

In the first instance the flow is considered isentropic. Ignoring real-gas effects the temperature T and density ρ are simply related by the isentropic relations for an ideal gas

$$\rho T^{-1/(\gamma-1)}=\text{const} \tag{4.1}$$

with γ the ratio of heat capacities at constant pressure and volume, $\gamma=c_p/c_v$. A relation between T and X, the position in the flow field, exists via the so-called Mach number M, the ratio of the flow velocity to the local sound velocity[29]

$$\frac{T}{T_0}=\left[1+\frac{\gamma-1}{2}M^2\right]^{-1} \tag{4.2}$$

with T_0 the source temperature. M is a function of X/D only, where D is the nozzle diameter. The temperature in an isentropic expansion, therefore, does not depend on the density. Expressions for M have been given in the literature.[29–31] As an example, for $X/D=2$ the temperature in an expansion of argon from a room-temperature source is approximately 36 K. The density is 0.042 times its value in the source.

In the case of expansions of molecules the very high cooling rates in the expansion are not always matched by an equal cooling of the internal degrees of freedom of the molecules. If relaxation between these degrees of freedom and the translational bath occurs at too slow a rate, the occupations of the states of the molecules may differ markedly from the Boltzmann distribution expected at the temperature of the translational bath.[28,32] Therefore, in the expansions we have studied, it is not *a priori* clear what the occupations of the dimer states will be. Intensity measurements in the Raman spectra can give quantitative information pertaining to this distribution.

As the gas expands the total particle density rapidly falls but the dimer fraction increases due to the decreasing temperature. An optimum in the dimer signal was, therefore, found experimentally. Most of the measurements were taken near this optimum which was located at $X/D\simeq 2$. Slightly downstream of the optimum the dimer signal disappeared below our detection limits. This was partly due to a massive clustering in the expansion, which will be discussed in the accompanying article.

V. DIMER SPECTRA

In this section we present the measured dimer spectra. First, a comparison is made with the earlier spectroscopic work. In the second part of this section the intensities of the spectra are compared to the predictions of Sec. II.

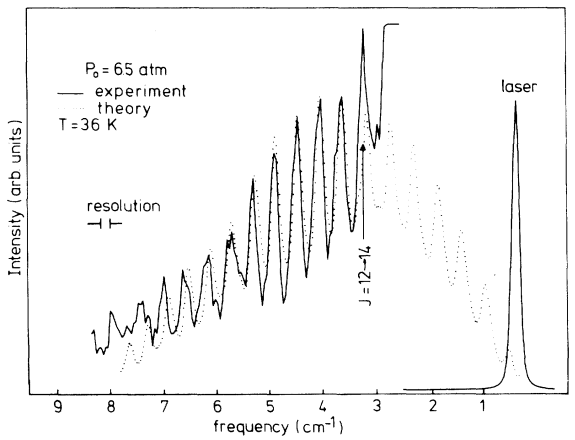

FIG. 3. Low-resolution Raman spectrum of the Ar_2 pure rotational transitions. Source pressure $p_0=6.5$ atm. Distance from nozzle $X/D=2.0$. Theoretical spectrum was calculated using the DID model. Temperature as determined from the spectrum is $T=36\pm 8$ K. This was equal within experimental uncertainty to the temperature determined with a seeding technique (see paper II): $T_{\text{seed}}=39\pm 1.2$ K.

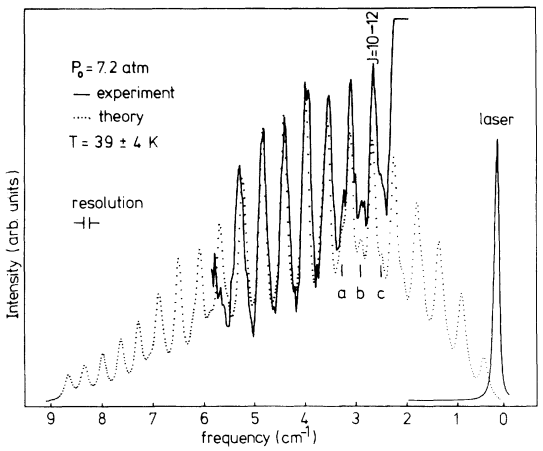

FIG. 4. High-resolution rotational Raman spectrum of Ar_2, showing hot ($v=1$) transitions (indicated by *a*, *b*, and *c*). Expansion conditions were as in Fig. 3. Temperature as determined from the spectrum is again given in the figure and $T_{seed}=39.3\pm0.8$ K.

A. Spectroscopy

1. Rotational spectra

Pure rotational spectra of Ar_2 were recorded with frequency shifts between ~ 8 and 2 cm^{-1}. A low-resolution (0.18-cm^{-1}) spectrum is shown in Fig. 3. The peaks in the spectrum correspond to transitions of molecules in the ground vibrational state. Attempts to observe transitions at frequency shifts larger than 8 cm^{-1} were unsuccessful due to the weakness of the signal; at frequencies smaller than ~ 2 cm^{-1} the laser interference was too large.

A high-resolution (0.09-cm^{-1}) rotational spectrum recorded with approximately the same expansion conditions as in Fig. 3 is shown in Fig. 4. To obtain a high signal-to-noise ratio only part of the spectrum was scanned, enabling longer measurement times per data point. In addition to the main peaks, smaller intermediate features (labeled *a*, *b*, and *c*) are seen that arise from transitions in "hot" molecules in the first excited vibrational state.

By recording several spectra similar to the ones shown in Figs. 3 and 4 it was possible to determine the transition frequencies and check the reproducibility of the system. In general, it was found that peak positions (i.e., frequencies of transitions) reproduced to approximately ± 0.03 cm^{-1} in successive runs on one day. Differences in frequencies between successive transitions also reproduced to about 0.03 cm^{-1} between runs on different days, however, the peak positions did not reproduce very well. This was due to the nonlinear response of the piezoelectric transducers, discussed in Sec. III. A different bias voltage after the daily initial alignment would change the average linear response of the system and thereby its frequency calibration. The nonlinearity is seen, e.g., in Figs. 3 and 4 where the laser position does not coincide exactly with the zero of the abscissa. The calibration procedure outlined in Sec. III was, therefore, indispensable for determining the transition frequencies and identifying the lines.

Very good agreement exists between our results and those of CD.[9] This is shown in Table II where measured Raman transition frequencies are given together with the ones calculated from CD. Note that we could not measure the frequency with good absolute accuracy, so the frequency of the $J=16\rightarrow 18$ transition was fixed to the value of CD and all the others were derived from it. Although the resolution obtained in this experiment is higher than in the CD experiment, the very large amount of data makes their results more accurate than ours. A further test of the accuracy of the results is found by calculating differences ($\Delta\nu$) in the frequencies of successive lines. The smooth behavior of the CD results is not completely reflected in our results since the scatter is larger. Although there is, in general, good agreement between our results and those of CD, there are still some small deviations that are not entirely due to scatter. This is seen for the difference frequency $\nu(16\rightarrow 18)-\nu(14\rightarrow 16)$ which is considerably smaller than the result of CD (0.42 instead of 0.45 cm^{-1}). As a consequence, the lowest two measured frequencies are shifted with respect to the CD results. How this would affect the dimer levels cannot be concluded from these data since the choice of fixing the frequency of the $J=16\rightarrow 18$ transition at 4.00 cm^{-1} was made arbitrarily. In conclusion, our results confirm the analysis of CD in a direct manner for the levels observed in the experiment. Our observations are thus in good agreement with the predictions from the interatomic potential.[11]

2. Vibrational spectra

Vibration-rotation spectra were recorded in the optical bypass system discussed in Sec. III. Since we expected a signal approximately 50 times weaker than for the case of the pure rotational spectra, we did not try to resolve individual vibrational-rotational transitions. Therefore, the peaks in the vibrational-rotational spectrum (Fig. 5) correspond to unresolved transitions close to the bandheads of some of the vibrational-rotational bands. In the theoretical spectrum (to be discussed below) they are labeled by S and Q for $\Delta J=+2$ and 0, respectively. Subscripts indicate the initial vibrational states. At

TABLE II. Comparison of present spectroscopic results with results of Colbourn and Douglas (Ref. 9) for pure rotational Raman transitions in ground vibrational Ar_2 molecules. Column 1: initial and final rotational quantum numbers. Column 2: Raman transition frequency calculated from results of Ref. 9 in cm^{-1}. Column 3: present measurements. Column 4: differences in transition frequencies calculated from column 2. Column 5: differences in transition frequencies calculated from column 3. Transition frequencies 16→18 are arbitrarily set equal to each other in columns 2 and 3.

	ν		$\Delta\nu$	
Transition $J \rightarrow J'$	CD (Ref. 9)	This work average	CD (Ref. 9)	This work
0→2	0.35		0.46	
2→4	0.81		0.46	
4→6	1.27		0.45	
6→8	1.72		0.43	
8→10	2.19		0.46	
10→12	2.65	2.67±0.01	0.44	0.46
12→14	3.09	3.13±0.01	0.46	0.45
14→16	3.55	3.58±0.01	0.45	0.42
16→18	4.00	4.00	0.44	0.44
18→20	4.44	4.44±0.01	0.44	0.45
20→22	4.88	4.89±0.02	0.43	0.41
22→24	5.31	5.30±0.03	0.44	0.41
24→26	5.75	5.71	0.41	0.45
26→28	6.16	6.16	0.43	0.41
28→30	6.59	6.57	0.41	0.43
30→32	7.00	7.00	0.41	0.41
32→34	7.41	7.41	0.36	
34→36	7.77			

this point it is also anticipated that the O branches ($\Delta J = -2$) are smoothed out so as to give no observable peaks in the spectrum. As seen in Fig. 5 only S_0 and S_1 peaks were observed with $\Delta v = 1$. The S_0 peak position was found to be 28.0±0.3 cm^{-1}, in agreement with the position calculated from the results of CD. However, the S_1 peak was shifted up in frequency by about 0.8 cm^{-1} relative to the calculated position. Different weighting of the individual transitions that contribute to the peak intensity can-

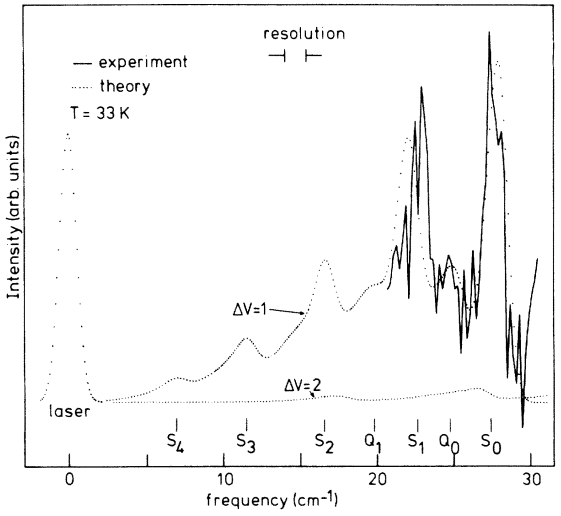

FIG. 5. Low-resolution rotation-vibration spectrum over a limited frequency range. Intensities are about a factor of 100 smaller than in the pure rotation spectra, Figs. 3 and 4. Temperature as given in the figure was determined from seeding.

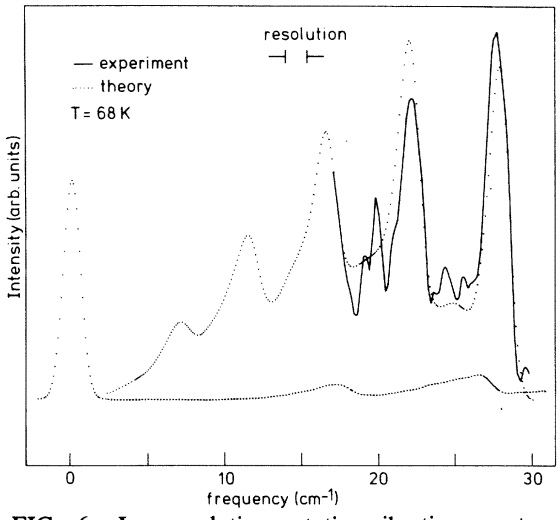

FIG. 6. Low-resolution rotation-vibration spectrum over a limited frequency range. High-temperature spectrum was recorded at the University of Nijmegen.

TABLE III. Matrix elements of different diatom anisotropic polarizability models for Ar_2. Matrix elements shown are calculated for transitions $v=0$, $J=0\rightarrow v'=0,J'=2$. Column 2: analytical form of model function. Column 3: reference and equation number. Column 4: calculated matrix elements.

Model No.	Model function	Ref., Eq.	Matrix element (a.u.)
1	$6\frac{\alpha_0^2}{\sigma^3}\left[\frac{\sigma^3}{R^3}+\alpha_0\frac{\sigma^3}{R^6}\right]$	DID[a]	2.02
2	$6\frac{\alpha_0^2}{\sigma^3}\left[\frac{\sigma^3}{R^3}-0.289\frac{\sigma^5}{R^5}\right]$	Ref. 33, Eq. (3)[a]	1.50
3	$6\frac{\alpha_0^2}{\sigma^3}\left[\frac{\sigma^3}{R^3}-0.473\frac{\sigma^{9.3}}{R^{9.3}}\right]$	Ref. 33, Eq. (4)[a]	1.48
4	$6\frac{\alpha_0^2}{\sigma^3}\left[\frac{\sigma^3}{R^3}-0.226\frac{\sigma^{6.5}}{R^{6.5}}\right]$	Ref. 33, Eq. (5)[a]	1.65
5	$6\frac{\alpha_0^2}{\sigma^3}\left[\frac{\sigma^3}{R^3}-0.330\frac{\sigma^{11.1}}{R^{11.1}}\right]$	Ref. 33, Eq. (6)[a]	1.68
6	$6\alpha_0^2\left[R^{-3}-0.107a_0^{-3}\exp\left[\frac{-R}{2.36a_0}\right]\right]$	Ref. 33, Eq. (7)[b]	−1.71
7	$6\alpha_0^2R^{-3}-1.28\alpha_0^2\frac{a_0^{1.12}}{R^{4.12}}$	Ref. 33, Eq. (8)[b]	1.91
8	$6\alpha_0^2R^{-3}-1162a_0^3\exp\left[\frac{-R}{0.901a_0}\right]$	Ref. 33, Eq. (10)[b]	1.56
9	$6\alpha_0^2R^{-3}-3995a_0^3\exp\left[\frac{-R}{0.65a_0}\right]$	Ref. 34, Eq. (5), Table I[b]	1.89

[a] $\sigma=6.435$ a.u.

[b] a_0 is Bohr radius, $a_0=1$ a.u. $=0.529\,177$ Å.

not resolve the discrepancy since the peak extends well beyond the bandhead indicated by CD. In order to check this result experiments were subsequently repeated at the University of Nijmegen where a similar intracavity system with approximately ten times more laser power is available. The higher power enabled us to obtain a better signal-to-noise ratio in the spectra. Results for runs with a sonic nozzle of 250 μm diameter are shown in Fig. 6. The S_1 peak position was repeatably found at 22.1 ± 0.3 cm^{-1}, in agreement with CD. The discrepancy with the previous measurement remains unresolved.

B. Intensities

1. *Rotational spectra*

With the use of the results of Sec. II and with a knowledge of ρ_{vJ}, the density of dimers in the state $|vJ\rangle$, it is possible to calculate a theoretical spectrum which can be compared with experiment. The assumption was made that the distribution over the dimer states is thermal, so that

$$\rho_{vJ}\propto g_J e^{-E_{vJ}/kT}$$

with g_J the degeneracy and E_{vJ} the energy of the level v,J. The temperature T need not be equal to the local translational temperature as calculated with Eq. (3.2). With this assumption, spectra were synthesized by smoothing over the instrumental line-shape function. As shown in Sec. II this determined the overall line shape for all of the important transitions. Through variation of the temperature, theoretical curves were fitted to the observed spectra to within experimental error as shown in Figs. 3 and 4. Fitted temperatures are also indicated there. Other fitting parameters were the absolute intensity and a smoothly varying background due to laser stray light and photomultiplier dark count. In Fig. 4 also the intensities of the $v=1$ hot band transitions (denoted by *a*, *b*, and *c*) are predicted to within the experimental uncertainty by the DID model and the assumption of a thermal distribution.

Until now only the DID model was discussed.

Several different polarizability models were also tried in the fitting procedure. These analytical models are given in Ref. 33, Eqs. (3)—(8) and (10) and Ref. 34, Eq. (15) and Table I. The polarizability in these models differs significantly from the result of the DID model. This is seen in Table III where the matrix elements are given, calculated with the different models. However, since the dimer wave functions probe only a limited range of internuclear distances ($6.4 < R < 9.0$ a.u.) inside the potential well, the fractional changes in the matrix elements are fairly independent of the dimer states involved in the Raman transition. Therefore, the quality of the fitting was not significantly affected. In view of the results of Refs. 16--18, the simple DID model was therefore used in the fits to the observed spectra. On the other hand, it was not possible to rule out these models on the basis of the spectra alone. In the companion article we shall return to this question. Independent of the model that was used for the polarizability, it can now be concluded that the assumption of a thermal distribution over the rotational levels is good. From the absence of hot bands in the spectra (other than $v=1$), limits on the occupation of the higher excited states can be set. Since these level occupations are determined by the kinematics of the expansion this will be treated in paper II. Independent measurements of the temperature by means of a seeding technique will also be discussed there. At this point it is only mentioned that the two temperature determinations, from the Ar_2 spectra and from seeding, agreed to within experimental error.

2. *Vibrational spectra*

A somewhat different procedure was used to compare the vibrational spectra to theory. Because of the low signal-to-noise ratio we did not attempt to determine the temperature from the spectra. Instead, a measurement of the temperature by means of the seeding technique was used in the calculation of the vibrational spectra. The calculated spectra were again smoothed with the instrumental line shape. The adjustable parameters in this case were the background and the intensity. Since two peaks were measured, only the ratio of their heights is now of significance in judging the quality of agreement between theory and experiment. The theoretical curves (Fig. 5) for both the $\Delta v=1$ and $\Delta v=2$ transitions are shown separately. At the frequencies of observation the $\Delta v=2$ transitions give rise to an almost structureless background of low intensity. At frequencies between 35 and 50 cm^{-1} its contribution is not negligible, however, and in future experiments it should be possible to observe these transitions.

VI. SUMMARY OF RESULTS

Under conditions of high-density flow it was possible to observe Raman scattering from ground electronic state argon dimers. The observed transition frequencies in the rotational spectra agreed within the experimental error with vacuum-ultraviolet absorption measurements of Colbourn and Douglas. The intensity of those transitions could be explained under the assumption of a classical point-dipole-induced dipole model for the polarizability and a thermal distribution of the dimers over the rotational states with $v=0$ and $v=1$. The much weaker vibrational transitions were also observed. Their position was also found to be in agreement with the results of Colbourn and Douglas. These results establish the technique of studying dimers by Raman scattering in a supersonic expansion as reliable and of potential use in studying a variety of dimer systems.

ACKNOWLEDGMENTS

We thank G. M. van Waveren for assistance with the measurements and G. Luijks of the University of Nijmegen for performing some measurements of vibration spectra. Discussions with Dr. A. Lagendijk and Dr. D. Frenkel were very useful. The financial support of the Stichting Fundamenteel Onderzoek der Materie is gratefully acknowledged.

---

*Address after 1 September 1982: Lyman Laboratory of Physics, Harvard University, Cambridge MA 02138.

[1]E. W. Becker, K. Bier, and W. Henkes, Z. Phys. 146, 333 (1956).

[2]P. G. Bentley, Nature 190, 432 (1961); W. Henkes, Z. Naturforsch. 16a, 842 (1961).

[3]O. F. Hagena, in *Molecular Beams and Low Density Gas Dynamics*, edited by P. P. Wegener (Dekker, New York, 1974), Ch. 2.

[4]See, e.g., J. A. Beswick and J. Jortner, in *Advances in Chemical Physics*, edited by J. Jortner, R. D. Levine, and S. A. Rice (Wiley, New York, 1981), Vol. 47, p. 363, and references therein.

[5]H. P. Godfried and I. F. Silvera, Phys. Rev. Lett. 48, 1337 (1982).

[6](a) C. E. Morgan and L. Frommhold, Phys. Rev. Lett. 29, 1053 (1972), reported the observation of an unresolved rotational band of Ar_2. Subsequently, their observations could not be repeated with improved apparatus. Their claimed observation was attributed to

an instrumental effect; (b) L. Frommhold, K. H. Hong, and M. Profitt, Mol. Phys. 35, 665 (1978).
[7]L. Frommhold, J. Chem. Phys. 61, 2996 (1974).
[8]Y. Tanaka and K. Yoshino, J. Chem. Phys. 53, 2012 (1970).
[9]E. A. Colbourn and A. E. Douglas, J. Chem. Phys. 65, 1741 (1976).
[10]G. C. Maitland and E. B. Smith, J. Chem. Eng. Data 17, 150 (1972).
[11]R. A. Aziz and H. H. Chen, J. Chem. Phys. 67, 5719 (1977).
[12]P. v. d. Kam, Ph.D. thesis, Technical University of Eindhoven, 1981 (unpublished).
[13]G. Placzek, in *Handbuch der Radiologie,* edited by E. Marx (Akademische, Leipzig, 1934), Vol. 6, Pt. II.
[14]No alignment of the molecules in the expansion is assumed here.
[15]J. P. MacTague, W. D. Ellenson, and L. H. Hall, J. Phys. (Paris) Colloq. 33, C1-241 (1972); P. Lallemand, Phys. Rev. Lett. 25, 1079 (1970); H. B. Levine and G. Birnbaum, J. Chem. Phys. 55, 2914 (1971); A. D. Buckingham and D. A. Dunmur, Trans. Faraday Soc. 64, 1776 (1968), determined the anisotropy from second virial Kerr coefficient measurements.
[16]L. Frommhold, in *Advances in Chemical Physics,* edited by I. Prigogine and S. A. Rice (Wiley, New York, 1981), Vol. 46.
[17]D. P. Shelton and G. C. Tabisz, Can. J. Phys. 59, 1430 (1981).
[18]K. L. Clarke, P. A. Madden, and A. D. Buckingham, Mol. Phys. 36, 301 (1978).
[19]D. W. Oxtoby and W. M. Gelbart, Mol. Phys. 30, 535 (1975).
[20](a) A. D. Buckingham, Trans. Faraday Soc. 52, 1035 (1956); (b) A. D. Buckingham and K. L. Clarke, Chem. Phys. Lett. 57, 321 (1978).
[21]L. Frommhold and R. Bain, J. Chem. Phys. 63, 1700 (1975).
[22]J. M. Parson, P. E. Siska, and Y. T. Lee, J. Chem. Phys. 56, 1511 (1972).
[23]In Ref. 21 the factor of 0.6639 $Å^3$ in the asymptotic expression for the point DID model should have been 0.4290 $Å^3$.
[24]D. Frenkel and J. P. MacTague, J. Chem. Phys. 70, 2695 (1979).
[25]R. G. Gordon, Adv. Magn. Reson. 3, 1 (1968).
[26]L. I. Schiff, *Quantum Mechanics* (MacGraw-Hill, New York, 1955).
[27]R. J. Le Roy and W.-K. Liu, J. Chem. Phys. 69, 3622 (1978); R. J. Le Roy and R. B. Bernstein, J. Chem. Phys. 54, 5115 (1971).
[28]I. F. Silvera and F. Tommasini, Phys. Rev. Lett. 37, 136 (1976); I. F. Silvera, F. Tommasini, and R. J. Wijngaarden, *Rarefied Gas Dynamics, Progress in Astronautics and Aeronautics,* edited by J. L. Potter (AIAA, New York, 1977), Vol. 51, Pt. II, p. 1295.
[29]J. B. Anderson, in *Molecular Beam and Low Density Gas Dynamics,* edited by P. P. Wegener (Dekker, New York, 1974), Ch. 1.
[30]P. L. Owen and C. K. Thornhill, Aeronautical Research Council (United Kingdom) Report No. RM-2616, 1948 (unpublished).
[31]H. Ashkenas and F. S. Sherman, *Proceedings of the Fourth International Symposium on Rarefied Gas Dynamics, Toronto, 1964,* edited by J. H. de Leeuw (Academic, New York, 1966), Vol. 2, p. 84.
[32]H. P. Godfried, I. F. Silvera, and J. van Straaten, *Rarefied Gas Dynamics, Progress in Astronautics and Aeronautics,* edited by S. S. Fisher (AIAA, New York, 1981), Vol. 74, Pt. II, p. 772.
[33]L. Frommhold and M. H. Profitt, Mol. Phys. 35, 681 (1978).
[34]M. H. Profitt, J. W. Keto, and L. Frommhold, Can. J. Phys. 59, 1459 (1981).